Electric Power Systems Research 196 (2021) 107188

Contents lists available at ScienceDirect

Electric Power Systems Research

journal homepage: www.elsevier.com/locate/epsr

PMU-voltage drop based fault locator for transmission backup protection

Jose J. Chavez [a], Nidarshan Veera Kumar [b], Sadegh Azizi [d], Jose L. Guardado [a], Jose Rueda [b], Peter Palensky [b], Vladimir Terzija [c], Marjan Popov [b,*]

[a] The Graduate Program and Research in Electrical Engineering, National Technological Institute of Mexico Campus, Morelia 58120, Mexico
[b] Delft University of Technology, Faculty of EEMCS, Mekelweg 4, Delft, 2628CD, the Netherlands
[c] Skolkovo Institute of Science and Technology, Bolshoy Boulevard 30, bld. 1, Moscow 121205, Russia
[d] School of Electronic and Electrical Engineering University of Leeds, Leeds, United Kingdom

ARTICLE INFO

Keywords:
Phase measurement unit
Wide-area fault location
Least-square technique
Delta current method
RTDS

ABSTRACT

Local protection elements such as fuses and relays are the first protective mechanism to clear the fault and isolate the affected part of the power grid. Although the selectivity, speed, and sensitivity of these primary protection devices are relatively high, they cannot be considered flawless. There is a small percentage of events for which relays experience blinding effects. For these scenarios, a redundant arrangement can be made through backup protection. This paper proposes a centralized remote backup protection method based on two techniques, the delta algorithm and the least-squares technique. The proposed method successfully detects the faulted transmission line, fault type, and the distance to the fault. Besides, it makes use of phasor measurement unit data and it is non-iterative. The grid is split in a user-determined number of subareas based on the phasor mesurement unit locations, in order to accurately determine the fault location. Firstly, the faulty area is located and thereafter an in-depth search is carried out on the faulted area to determine the faulted line. Finally, the fault distance is determined based on the distributed parameter model of the transmission line. The method is demonstrated and validated in an RTDS-Matlab co-simulation platform. Extensive simulation studies are carried out on the IEEE 39-bus system to validate the proposed method.

1. Introduction

Backup protection plays an important role in preventing and mitigating failure effects of equipment and primary protection schemes. Backup protection operates because it is intentionally set to meet specific performance requirements or because multiple contingencies have occurred in the system leading the event to the backup protection zone. Back up protection may be operated locally, remotely, or both.

To realize the remotely operated backup protection, the use of phasor measurement unit (PMU) data has been the focus of academia and industry for several years. In power system protection, the PMU data were first used for fault detection and location. In [1] and [2], PMU data were implemented for system-wide fault diagnosis and location. The PMU data without post-processing for online estimation were used in [3], whilst the use of a Markov-based probabilistic approach and PMU data for fault location was proposed in [4].

Recently, the PMU data-driven methods were presented for wide area backup protection (WABP) [5], with an execution time which is typically longer than that of the primary protection. These methods are generally based on current data provided by the current transformer's outputs, which can adversely affect the accuracy of the result. Therefore, the use of a bus admittance matrix and measured voltages was proposed in [6]. Furthermore, PMU-based algorithms can deal with signals with higher-order harmonic contents, which are needed for fault detection, location and discrimination, as reported in [7].

WABP algorithms based on PMU data are characterized as highly accurate for fault location, thus improving the performance of protection schemes [8]. For some schemes, the accuracy depends on the number and the location of PMUs deployed in the system [9]. As networks are normally not fully observable, a fault-location algorithm

This work was financially supported in part by CONACyT-SENER energy sustainability PE-A-03 and by the Dutch Scientific Council NWO-TTW, under the project 647.003.004 "Resilient Synchro-phasor Grid Protection Platform (ReSident)". Paper submitted to the International Conference on Power Systems Transients (IPST2021) in Belo Horizonte, Brazil, June 6–10, 2021.

* Corresponding author.
E-mail addresses: jose.cm@morelia.tecnm.mx (J.J. Chavez), N.K.VeeraKumar@tudelft.nl (N.V. Kumar), s.azizi@leads.ac.uk (S. Azizi), jose.gz@morelia.tecnm.mx (J.L. Guardado), J.L.RuedaTorres@tudelft.nl (J. Rueda), P.Palensky@tudelft.nl (P. Palensky), v.terzija@skoltech.ru (V. Terzija), M.Popov@tudelft.nl (M. Popov).

https://doi.org/10.1016/j.epsr.2021.107188
Received 31 October 2020; Received in revised form 19 March 2021; Accepted 22 March 2021

based on fewer PMU measurements in large scale transmission networks has been proposed in [10-13]. It is also known that PMU data can be erroneous or lost on their way to the control room. Therefore, some techniques that deal with data corruption issues are proposed in [14-18]. Ahead of the growing use of synchrophasor and storage data, smart techniques are being offered for the early detection of single/-multiple faults and clustering [18, 19]. In addition, some methods can handle synchronized and unsynchronized data giving flexibility in the sampling data collection [20].

This paper addresses the topic of WABP by early fault detection and identification. The method is based on two techniques, namely the delta algorithm and the least-squares estimator. The techniques are modified to work with a limited number of synchronized voltage and current data. The method is partitioned in three steps giving the possibility to use data from other intelligent electrical devices (IED) with different protocols and time stamp. The proposed method successfully locates the faulted line by identifying the fault type and calculates the fault distance within the local backup protection time limits. The main contributions of the paper are:

- Fault detection and phase selection methods, which make use of voltage phasor data. The principle of the method is the delta-current time value.
- A least-squares technique is used for fault location. In this paper, the method makes use of the positive sequence voltage and current phasors only. This significantly reduces the computational burden compared to the technique reported in [17].
- A power swing detection, which makes use of current phasor data. The method is based on the incremental current over time.
- The entire scheme is implemented in an RTDS environment and can be used as a benchmark for real-time simulation of future networks.

The methodology is presented in Section 2, where the implementation is clearly explained. This method has demonstrated advantages such as low computational burden, low memory requirements and high sensitivity with respect to signal changes. These characteristics facilitate its implementation in a real-time environment. Section 3 deals with implementing the method in real-time environment by using software in the loop (SiL) that virtually represents a control room. The applicability of the proposed method is tested on IEEE-39 bus system for approximately 756 fault cases.

2. Proposed methodology

The proposed method is divided in three main computation stages. These stages are related to the amount of power system elements under analysis, as shown in Fig. 1. The stages comprise the full network, the faulty area, and the faulted line. The first stage uses the PMU data taken from the full network. Here, a modified Delta Current Method (DM) [21], is applied to determine the faulted subarea by means of voltage data. The predefined subareas depend on the PMU location. The second stage focuses on the faulty area analysis. The faulted subarea should be fully observable by the intelligent electrical devices (IED) or PMU equipment. Measured current and voltage phasors are used in the set of linear equations, which define the standard linear model. Thus, the least-squares estimation method is applied to obtain the unbiased unknown variables and its corresponding residuals. By using the resulting least-squares residuals, the faulted line is identified. The third stage determines the line fault distance by using the distributed-parameter line model. The three stages are fully described in the next sections. Although the PMU location, or area partition, can be done randomly without no physical restrictions, it is recommended to partition the grid in nodes where more than two lines are connected.

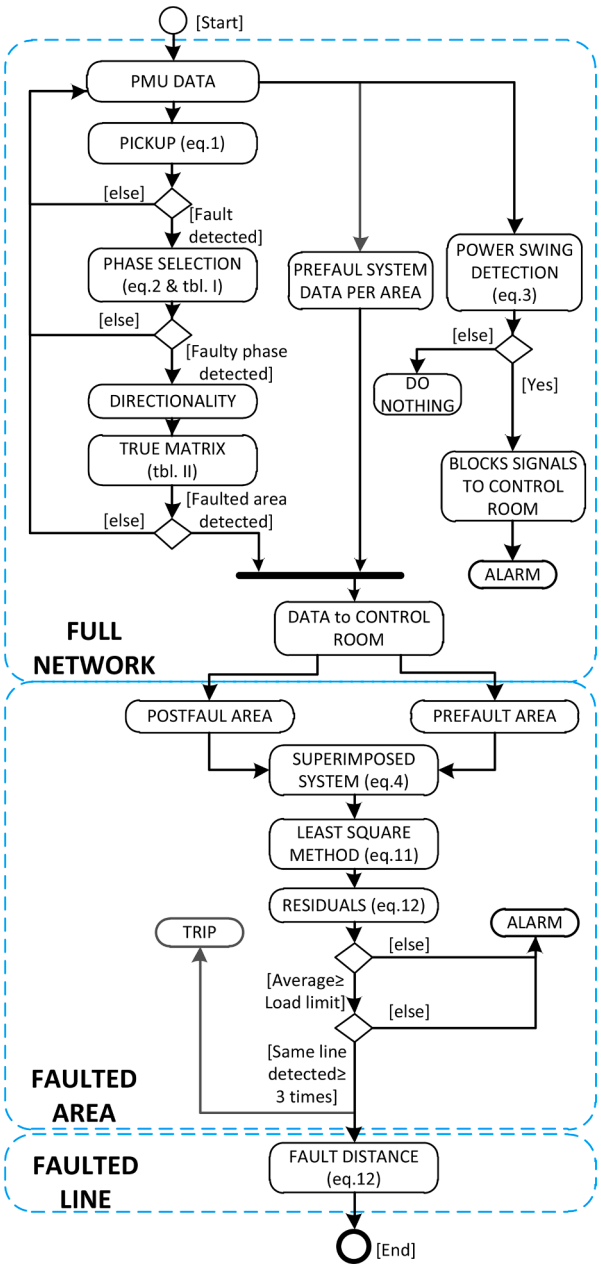

Fig. 1. Flowchart methodology break in steps.

2.1. First stage: full network

At this stage, the faulted area is detected. A modified DM is used as an event and a fault detection module. This step is performed for any boundary bus in the system equipped with a PMU. Usually, the DM takes actual current data. In this work, the actual phasor voltage is compared to a previous phase voltage using Euler's numerical differentiation [22]

$$\Delta V^{k}_{(n+1)A,B,C} = \frac{1}{\Delta t}\left(V^{k}_{(n+1)A,B,C} - V^{k}_{(n)A,B,C}\right) \quad (1)$$

Where $V^{k}_{(n+1)A,B,C}$, and $V^{k}_{(n)A,B,C}$correspond to the actual and previous values respectively, whilst Δt is the time step of the numerical solution. The previous voltage value represents the system in a steady condition. In this work, the previous value is the voltage phasor measured before the fault occurrence.

The disturbance is detected once the resulting is $\Delta V > 0.1/\Delta t$ (5% error plus a safety margin of 5%).

According to Fig. 1, the phase selection module is activated after the fault is detected. The faulty phase selection makes use of the delta method [23].

$$F_{TYPE} = round\left(\frac{\Delta V_A + \Delta V_B + \Delta V_C}{\max(\Delta V_A, \Delta V_B, \Delta V_C)}\right) \quad (2)$$

However, the technique is modified to work with the phasor voltage amplitude signals.

The involved number of phases in a fault is determined by (2). Furthermore, grounding faults are also detected by using the zero-sequence delta voltage phasors. By knowing F_{TYPE}, the zero-sequence, and by Table I, the faulty line is easily identified.

Once the faulty phase is detected, the directionality module takes place. In this work, the directionality module is computed according to [24] where the negative and zero sequence currents are used with a positive voltage polarization. The positive, negative and zero sequences are computed from the PMU data, and the signals have the same timestamp.

By the fault directionality module in at all the PMUs locations, the method can quickly determine the faulted area. An illustrative example is presented in Fig. 2. In the grid, 4 PMUs are used to split the system into three areas. Based on the fault direction and the truth table, the faulty subarea is easily located. The truth-table is a simple decision matrix, which is particular for any system and PMUs position. For instance, referring to Fig. 2, and current directions, truth-table is shown in Table II. The advantage of using a modified delta method and a modified fault selection module are the simplicity, fast detection and low computational burden.

As shown in Fig. 1, a power swing blocking module runs in parallel in this stage. The power swing (PS) detection is based on the continuous monitoring of the delta current [25]. For this purpose, the method is modified in order to make use of phasor quantities instead of time signals. The delta current (ΔI_{PS}) is calculated every cycle (0.016 s in 60 Hz or 0.02 s in 50 Hz system) by the following equation,

$$\Delta I_{PS} = \left|I_{Act} - I_{2cp}\right|, \quad (3)$$

where I_{Act} and I_{2cp} are the actual and two-cycle early current phasors respectively. A PS is detected when the ΔI_{PS} value increases by 5%, or more of the steady-state current phasor during three continuous cycles. The detection triggers the PS blocking and blocks the second stage of the method preventing a false trip (which occurs when the fault detection, phase selection, and directionality modules fulfill the criteria to produce a second stage trip command). The methodology presented in Fig. 3(a) shows the current signal depending on the time and Fig. 3(b) shows the corresponding phasor amplitude. The PS starts at 0.048 s, and it is detected at 0.08 s.

The continuous delta current detection method promptly detects a PS. We have to point out that PS detection is not the focus of this paper, and this algorithm is a supplement to the developed platform in order to avoid false tripping when power swing oscillations take place.

Table I
Faulty phase selection.

Fault	ΔV^0	F_{TYPE}	$\Delta V_{(A,B,C)}$
AG	1	1	$\Delta V_A > (\Delta V_B \vert \Delta V_C)$
BG	1	1	$\Delta V_B > (\Delta V_A \vert \Delta V_C)$
CG	1	1	$\Delta V_C > (\Delta V_A \vert \Delta V_B)$
ABG	1	2	$\Delta V_C < (\Delta V_A \vert \Delta V_B)$
BCG	1	2	$\Delta V_A < (\Delta V_B \vert \Delta V_C)$
CAG	1	2	$\Delta V_B < (\Delta V_A \vert \Delta V_C)$
AB	0	2	$\Delta V_C < (\Delta V_A \vert \Delta V_B)$
BC	0	2	$\Delta V_A < (\Delta V_B \vert \Delta V_C)$
CA	0	2	$\Delta V_B < (\Delta V_A \vert \Delta V_C)$
ABCG	1	3	–
ABC	0	3	–

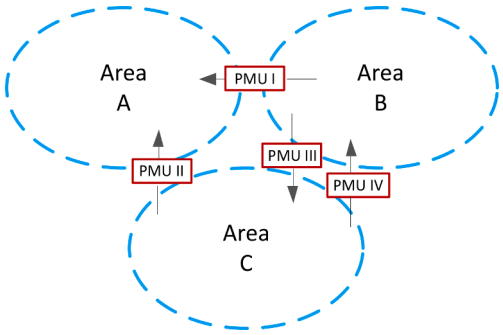

Fig. 2. Area partitioned by the use of PMUs localized at most representative buses.

Table II
Faulted area truth table.

AREA	PMU I	II	III	IV
A	F	F		
B	R		R	F
C		R	F	R

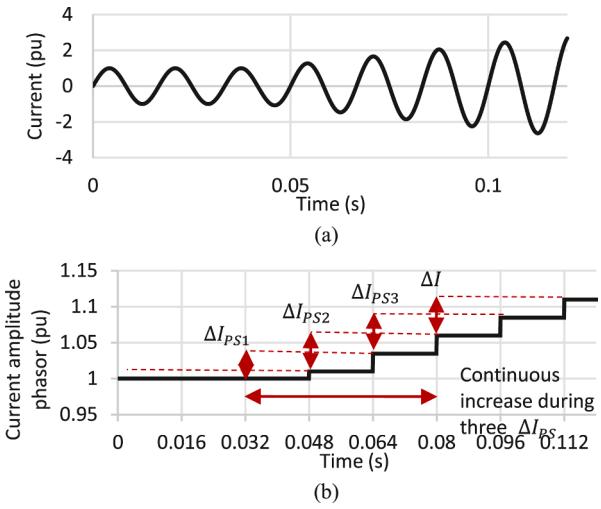

Fig. 3. Stable power swing (a) current signal and, (b) current phasor amplitude in both in pu.

2.2. Second stage: faulted area

The second computation stage deals with the faulted area to find the faulted line, as depicted in Fig. 1. This method is based on the superimposed values reported in [17, 18]; pre-fault and post-fault voltage and currents are collected from the system. Associated set of linear equations defines the wide area fault locator framework. The least-square technique solves the set of equations composed of the bus impedance matrices and the superimposed currents in all lines

. In this stage, only the positive sequence values are used. The pre-fault and post-fault nodal equations are expressed in (4) using the mesh current analysis.

$$V^{pre} = Z^{pre} I^{pre}; \quad V^{post} = Z^{post} I^{post}, \quad (4)$$

where I and V are the bus injected currents and the bus voltage phasors

from the system area in a vector matrix. The impedance matrix Z^{pre} and Z^{post} are the same, except for the rows and columns where the supposed faulted line *i–j* is located. The process is done for each of the lines in the subarea. The injected currents and voltage vectors of the faulted line *i–j* are replaced by two current sources as it can be seen in Fig. 4(a).

The nodal equation matrix resulting from the superimposed area (4) is

$$\begin{bmatrix} \Delta\overline{V}_1 \\ \vdots \\ \Delta\overline{V}_{Nf} \end{bmatrix} = -\begin{bmatrix} Z_{1,i}^{(i,j)} & Z_{1,j}^{(i,j)} \\ \vdots & \vdots \\ Z_{Np,i}^{(i,j)} & Z_{Np,i}^{(i,j)} \end{bmatrix} \begin{bmatrix} \Delta J_{i,j} \\ \Delta J_{j,i} \end{bmatrix} + \begin{bmatrix} Z_{1,1}^{(i,j)} & \cdots & Z_{1,Nb}^{(i,j)} \\ \vdots & \ddots & \vdots \\ Z_{Np,1}^{(i,j)} & \cdots & Z_{Np,Nb}^{(i,j)} \end{bmatrix} \begin{bmatrix} \Delta\overline{I}_1 \\ \vdots \\ \Delta\overline{I}_{Nb} \end{bmatrix}, \tag{5}$$

where *Np* is the number of total measured buses inside the area and *Nb* the area boundary terminals whit PMU. The superimposed measured phasor voltage for the *k*th bus is $\Delta\overline{V}_k = V_k^{post} - V_k^{pre}$ and the measured current phasor for the k_{th} line is $\Delta\overline{I}_k = I_k^{post} - I_k^{pre}$.

The measured data collected by PMUs may be corrupted due to some reasons, such as erroneous measurements, communication issues and external noise. Those effects are taken into account in the proposed method as errors between measured data and actual values. For every voltage on bus *k*, an error variable is added in (5a) ($e_v(k)$). Besides, the possible current measurement errors are integrated into the method as variables that should be accounted for (5b).

$$\Delta V_k^{meas} = \Delta\overline{V}_k + e_{v(k)}, \tag{6a}$$

$$\Delta I_k^{meas} = \Delta I_k + e_{I(k)}, \tag{6b}$$

The superimposed current of the sending end of line k can also be expressed in terms of the superimposed voltage when the distributed parameter line model equation is used. The superimposed voltages from (5) are used to obtain (6) as explained in [17, 18] .

$$\Delta J_k^{meas} = \sum_{q=1}^{Nb} C_{k,q}^{(i,j)} \Delta\overline{I}_q - C_{k,i}^{(i,j)} \Delta\overline{I}_{i,j} - C_{k,j}^{(i,j)} \Delta\overline{I}_{j,i} + e_{j(k)}, \tag{7}$$

where, *Jk* denotes the healthy line *k* sending-end current connected to terminals *u* and *w*. The parameter *C* is defined as

$$C_{k,q}^{(i,j)} = \frac{1}{Z_{u,w}^c}\left[\frac{Z_{u,q}^{(i,j)}}{\tanh(\gamma_{u,w} l_{u,w})} - \frac{Z_{w,q}^{(i,j)}}{\sinh(\gamma_{u,w} l_{u,w})}\right], \tag{8}$$

where lu,w, $Z^c u,w$ and $\gamma u,w$ refer to the line length, characteristic impedance and propagation constant, respectively. Thus, by using (5), the sending end currents are arranged in a set of two matrices, one with the suspicious line parameter *C* and another with the rest of healthy lines.

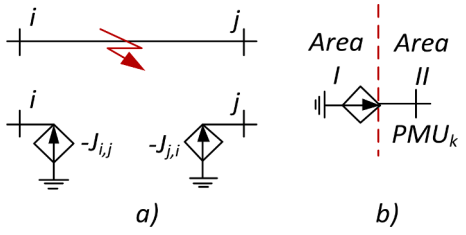

Fig. 4. Elements substitutions, *a*) transmission line and *b*) PMU between two areas.

$$\begin{bmatrix} \Delta J_1^m \\ \vdots \\ \Delta J_{Nh}^m \end{bmatrix} = -\begin{bmatrix} C_{1,i}^{(i,j)} & C_{1,j}^{(i,j)} \\ \vdots & \vdots \\ C_{Nh,i}^{(i,j)} & C_{Nh,j}^{(i,j)} \end{bmatrix} \begin{bmatrix} \Delta J_{i,j} \\ \Delta J_{j,i} \end{bmatrix} + \begin{bmatrix} C_{1,1}^{(i,j)} & \cdots & C_{1,Nb}^{(i,j)} \\ \vdots & \ddots & \vdots \\ C_{Nh,1}^{(i,j)} & \cdots & C_{Nh,Nb}^{(i,j)} \end{bmatrix} \begin{bmatrix} \Delta I_1 \\ \vdots \\ \Delta I_{Nb} \end{bmatrix}. \tag{9}$$

Where N_h is the number of healthy line terminals. The current phasors can be measured from a PMU or an intelligent device (IED) and used without any signal processing as long as the measurements have the same sampling and time synchronization.

Eqs. (6a), 6b), and ((9) are merged in a single matrix. This results in an overdetermined system.

$$\mathbf{M} = \mathbf{H}\mathbf{X} + e$$
$$\mathbf{M} = \mathbf{H}^J \begin{bmatrix} \Delta J_{i,j} \\ \Delta J_{j,i} \end{bmatrix} + \mathbf{H}^I \begin{bmatrix} \Delta I_1 \\ \vdots \\ \Delta I_{Nb} \end{bmatrix}, \tag{10}$$

where ***M*** and ***H*** denote the measurement vector and the coefficient matrix. The unknown superimposed current sources at the faulted line terminals are represented by ***X***.

By applying the least-squares method, the sets of unknowns are obtained from:

$$\widehat{\mathbf{X}} = (\mathbf{H}^*\mathbf{H})^{-1}\mathbf{H}^*\mathbf{M}. \tag{11}$$

Knowing that the voltage and current phasors are not sufficient to locate the faulted line. Therefore, the residuals are used as a faulted line locator.

$$\mathbf{r} = \mathbf{M} - \mathbf{H}\widehat{\mathbf{X}}. \tag{12}$$

The sum of the vector (***r***) is noticeably small for the faulted line set of equations. In this stage, the method does not need a threshold as the fault is detected in the previous stage.

2.3. Third stage: faulted line

For complete fault identification, the fault distance is computed in this stage. The fault location formula (13) is used at each of the superimposed sequence networks.

$$\alpha_{i,j} = \frac{\tanh^{-1}}{\kappa_{i,j}}\left(\frac{\cosh(\kappa_{i,j})\Delta V_j - Z_{i,j}^c \sinh(\kappa_{i,j})\Delta J_{j,i} - \Delta V_i}{\sinh(\kappa_{i,j})\Delta V_j - Z_{i,j}^c \cosh(\kappa_{i,j})\Delta J_{j,i} - Z_{i,j}^c \Delta V_i}\right), \tag{13}$$

where $\kappa_{i,j} = \gamma_{i,j} l_{i,j}$ and the voltage at the faulted line terminals ΔV_j and ΔV_j are derived from (8)

3. Methodology real-time implementation

The proposed methodology is tested on an RTDS- Matlab® co-simulation platform. The first stage and the electrical power system are developed in the Real-Time Simulation Software Package (RSCAD®). The PMU blocks are P-class library models which are developed according to IEEE C37.118 requirements. This stage is designed in a way to be implemented in local devices with a few modifications.

As it is supposed to be performed in a control room, the second part of the methodology is done by an external user work station. A GTNET card is used to interface the simulations, equipped with the transmission control protocol (TCP). The communication is bidirectional and asynchronous capable of sending up to 300 data points per package if

necessary. Fig. 5 shows the SiL scheme. It is seen that the RSCAD and Matlab PCs are connected to the real-time simulator RTDS by the local area network (LAN) switch, however with different channel and protocols. The TCP socket used in the second stage is connected to an external PC or two if necessary.

4. Study case

The proposed methodology is tested in IEEE-39 bus system. Fig. 6 represents the single line diagram where the PMU's locations are highlighted. Here, no sophisticated PMU placement method is required to split the network into different areas. However, it is recommended to allocate PMUs in the node where three or more lines are connected in order to separate the system. In this case, six PMUs are used to partition the system in 5 areas, demarcated by dashed lines in Fig. 6. The areas contain a similar number of elements, although the number of elements in each area should be settled following the user necessities.

Three RTDS racks with 5 PB5 run the system and the methodology in the first stage. In Fig. 6 the green line indicates which part of the system is allocated on racks 1 and 2. The third rack is used for assigning control elements. The simulation time-step is 50 μs. The PMUs reports at 240 frames/s with a latency of 200 μs. The RSCAD internally synchronizes the six PMUs data. The unique truth matrix used for this study case is shown in Table III. The first row has the PMU directional module, and forward and reverse faults are specified by F and R respectively.

4.1. Fault AB at 65% of line 4–14

Up to 756 different faults are simulated to test the accuracy of the method. However, only one case is presented and analyzed in detail. A line-to-line bolted AB fault at 65% of line 4–14 is analyzed in detail in this section. Firstly, the area of fault detection is found. In this case, the detection is realized at 0.0042 s as it can be seen in Fig. 7.

Although the delta algorithm is one of the fastest [21], the PMU reporting data of 240 frames per second adjusts the detection to 0.0042 s. The detection may seem slow compared to primary protection times, however, the presented methodology is intended to operate as backup protection.

According to transmission system operators, the backup protection system guidelines should operate from 400 ms to 600 ms. Fig. 7 shows the phasor voltages per phase at bus 4 and the corresponding memory voltage in solid and dashed lines, respectively. The fault is detected by almost all the PMUs with an accuracy inversely proportional to the fault distance.

In this case, the faulty phase is uncovered at 0.02 s after the fault inception. All the surrounding fault area PMUs successfully determine

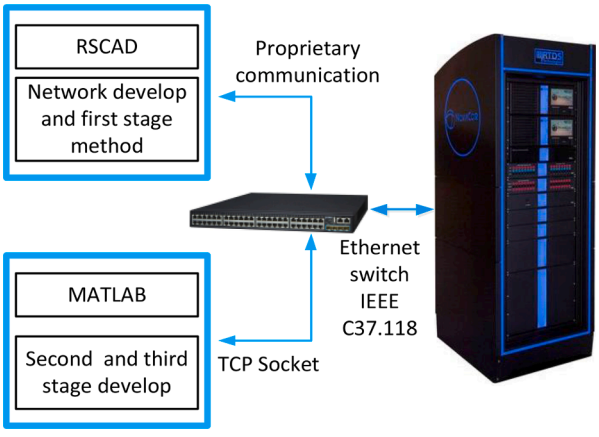

Fig. 5. Software in the loop (SiL) scheme using an RTDS, Transmission Control Protocol socket, LAN switch and externals PC.

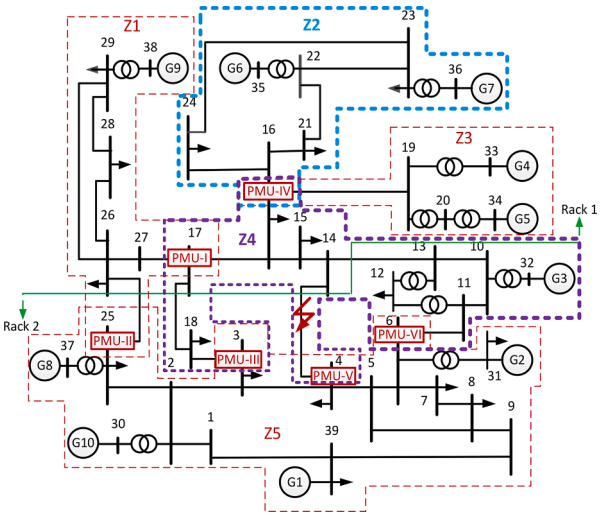

Fig. 6. IEEE 39 bus system whit a PMUs and the area partitioned.

Table III
Truth table for 39 bus system.

PMU	AREA				
	1	2	3	4	5
17–27	F			R	
25–26	F	F			R
16–24		F		R	
16–21			F	R	
16–19				R	
3–18				F	R
4–14				F	R
6–11				F	R

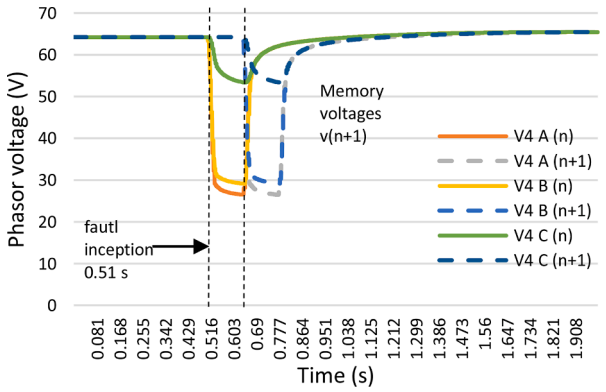

Fig. 7. Faulty phase detection during am AB fault at 65% of line 4–14.

the AB fault. Only phase AB is plotted in Fig. 8 the complete set of faulty phases are not included, however, the rest of the indicators remain inactive. The directionality is determined according to the resulting angles from positive and negative current sequence and positive voltage polarization. The direction characteristic angles should remain below $\pi/2$ rad and reverse angles from 1.83 to π rad during forwarding fault cases.

Fig. 9 shows that the angles from lines 3–18, 4–14, and 6–11 are in the forward zone while 17–27, 16–24, 16–21, and 16–19 in the reverse zone complying with the truth table column 4 of Table III. The square residuals are shown in Fig. 10(a) because this stage starts just after the faulty area detection. The square residuals before are equal to zero, and the counting time begins when the first stage is accomplished. During a fault condition, all the square residuals which correspond to the

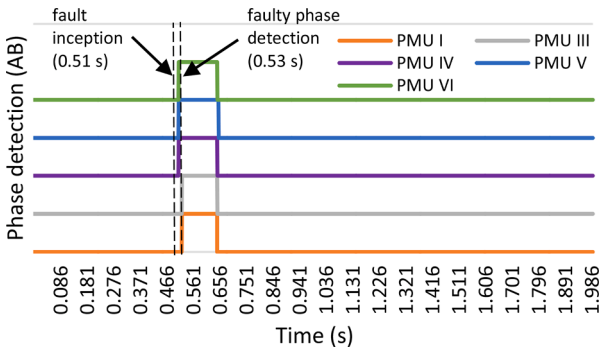

Fig. 8. Faulty phase detection during am AB fault at 65% of line 4–14.

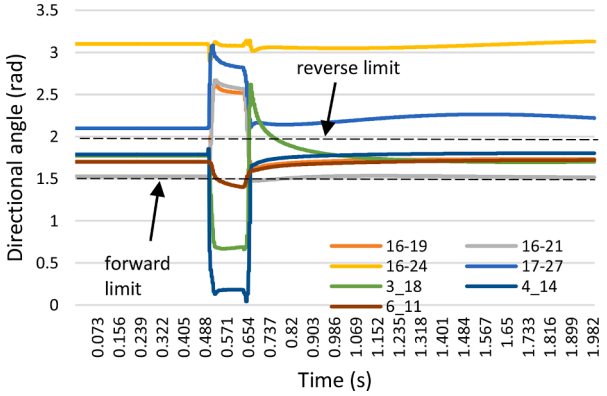

Fig. 9. Directional angles during a LL fault at 65% of line 4–14, in dashed lines the reverse and forward direction limits.

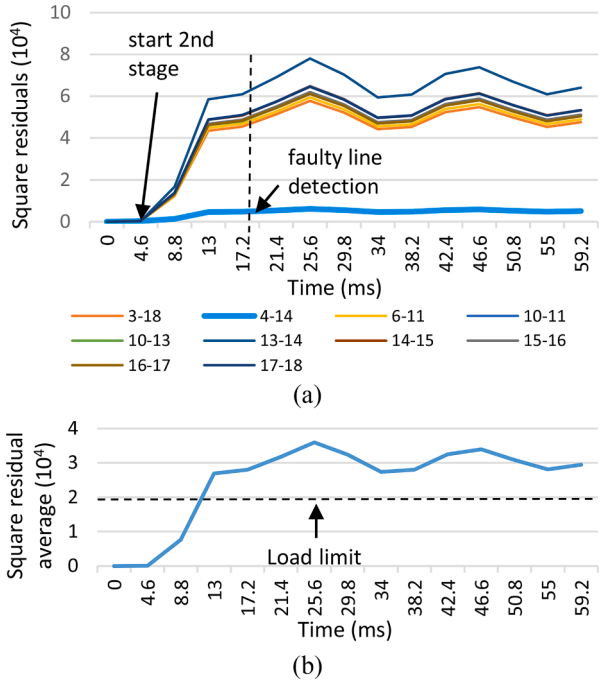

Fig. 10. Area 4, lines square residuals during an AB fault at 65% of line 4–14, (a) sum of squared residuals in all the suspected lines and (b) average between the lines maximum and minimum sum of square residuals.

suspicions lines will increase. Healthy lines show the most significant increase of the square residuals in comparison to the faulty lines. Thus, the detection of the faulty line can be quickly realized by magnitude comparison during the first three steps after the area detection. In this case, the fault is located at 63% of line 4–14 by using (11). The fault detection error is equal to 2% and only positive sequence is required. Thus, the computation memory in this stage is reduced by half compared to the proposed method in [12, 17].

4.2. Average detection times

The method is tested for 756 cases comprising three different lines, 4–14, 26–28, and 21–22; three fault distances 10%, 65%, and 90%; eleven fault types: AG, BG, CG, ABG, BCG, CAG, ABCG, AB, BC, CA, and ABC; three inception angles 0°, 45° and 90°; and apart from bolted faults, four fault resistances 0.1 Ω, 10 Ω, 50 Ω, and 75 Ω.

The average detection times are summarized in Table IV. All the times take zero as the fault inception. The fault detection, line detection, and distance detection comply with the PMU reporting times.

Because the simulation is done in a lab environment, the latency between the PMUs and the external software is negligible. The average accuracy in the distance fault detection is up to 97%.

4.3. Effect of high load switching

During peak load conditions, it is possible that the bus voltage drops significantly. Hence it can be erroneously seen by the protection schemes as a fault. Some backup schemes, especially those based on impedances, may trip the circuit. This is known as a relay trip on load encroachment. This can be considered as nuisance tripping, and it may even initiate cascading outages, leading to blackouts.

In order to prevent a false trip during switching of heavy loads, the proposed method uses a load-limit based on the average value of the minimum and maximum sum of the squared residuals. As explained in the flowchart of Fig. 1, the algorithm may activate stage 1 and enter in the second stage. On the contrary to a fault case, the sum of squared residuals (11) by transmission line does not show a noticeably small value. Thus the average value does not exceed the load limit. For the system study (see Fig. 6), the limit is fixed at 2×10^4 and is obtained by the following expression:

$$load - limit(k) = \frac{\max\left(r_{i-j}(k)\right) - \min\left(r_{i-j}(k)\right)}{2}. \tag{13}$$

The studied fault case presented in Fig. 10(b) shows that the average value surpasses the load-limit after a fault occurrence.

To test the load-limit, three different cases are simulated. In these cases, the load value of buses 15, 18, and 21 are triplicate and switched on to the system. As it can be seen in Fig. 11, the load-limit is surpassed for none of the cases. Thus, the method does not produce a trip signal.

4.4. Stable power swing cases

A stable PS case is simulated to test the performance of the PS blocking. In the IEEE 39 bus network, generators G9 and G3 are intentionally disconnected at the same time. This contingency gives rise to a stable PS for more than 10 s. The secondary voltage waveform is shown in Fig. 12(a) for a duration of 0.8 s (from 3.2 s to 4 s). Fig. 12(b) shows a zoomed-in view of the secondary current phasor increase. It can be seen that the ΔI is more than 5% of the steady-state current phasor and

Table IV
Average detection times in sec.

Fault detection	Phase detection	Direction	Area detection	Line detection	Fault distance
0.0042	0.0043	0.0045	0.0046	0.0172	0.025

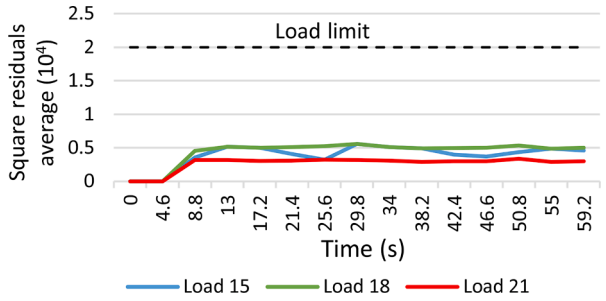

Fig. 11. Squared residuals average between maximum and minimum line values during high load switching at bus 15, 18, and 21.

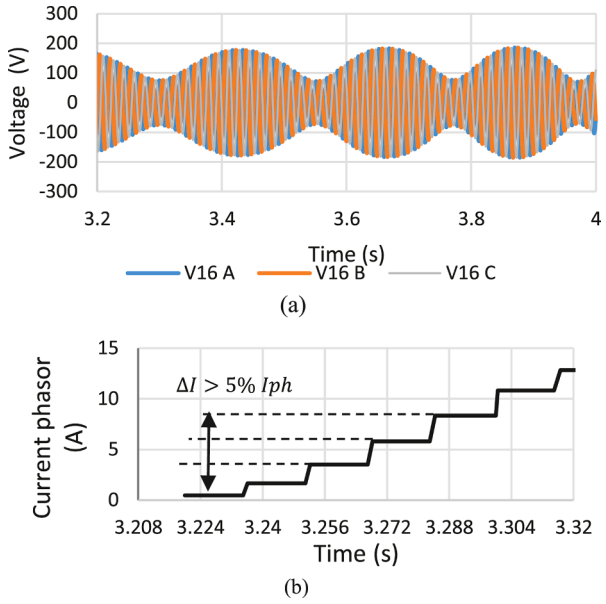

Fig. 12. Power swing case, (a) secondary time voltage and (b) secondary current phasor zoom-in.

gradually increases for more than three cycles. Thus, the swing phenomenon is detected by the PS module and triggers a blocking action to the second stage.

4.5. Comparison with existing backup protection schemes based on PMU data

The proposed method is compared with existing backup protection schemes that utilize synchrophasors data. The advantage of the method is that it can identify the faulted line by an arbitrary PMU location which so far was not possible in [5]. Also, the faulty phase is identified, and hence three poles or single-pole trip is allowed. The faulted lines are identified correctly within several milliseconds (in an average of 0.025 s using a reporting rate of 240 frames/s). The data protocol between stages can be mixed, simplifying the use of data from other intelligent devices. A brief comparison summary of the main characteristics of the schemes is shown in Table V.

5. Conclusions

This paper presents a method for backup protection in transmission systems using PMU data. The method detects the faulty line and phase and determines the fault direction and fault location. Hence, the presented method comprises three stages: faulty area location, faulty line location, and distance determination.

In the first stage, the proposed method combines different techniques already used in protection systems. However, those techniques are modified to work with voltage phasor data and have been optimized to decrease the computational burden. In the first module, the delta technique is modified to be applied to the phasor voltage drop. In the second module, the faulty phase selection is purely based on phasor voltage values. As a third module, the directionality is determined by making use of zero and negative sequence values in combination with the positive voltage polarization. In parallel, a module for power swing detection and blocking runs. The method uses the delta current phasors to determine a powers swing within three cycles. For the study case, power swings are detected in 0.048 s. After the detection, a blocking command is sent to the second stage preventing a false trip.

In the second stage, a reduced least-square method is applied to locate the faulted line by using the sum of the squares of the residuals. Only positive-sequence voltages and currents are required and hence the computational burden decreases in comparison to the method reported in [17]. At the end of this stage, the user already knows the faulted line, the faulty phase and the fault direction. In the third stage, the method computes the fault distance with an average accuracy of up to 97%.

The method has been successfully implemented in a real-time environment using SiL. The execution times depend on the size of each area. However, in this work, the reported average execution times are compatible with primary backup protection times. The method is not restricted to PMU data, as other IEDs data can also be used, as long as the data timestamp is synchronized to a common time reference. The method can potentially be used with different data protocols, one per stage. Also, it may detect more than one fault simultaneously in a different area.

The fault detection module is quite sensitive. It could be potentially used for high impedance faults and other events, which classical protection schemes cannot detect. For phenomena such as power swings, the proposed method prevents a false protection operation. The power swing aspect will be a challenging case. Power sings and high impedance fault events are beyond the scope of the paper and can be a topic for future research.

Table V
Performance comparison of backup based on PMU data.

Characteristic	[5]	[17] [23]	[20]	[18]	proposed
PMU data loss	No	some	some	some	some
Iterative solution	No	No	Yes	No	No
Computational burden	Low	Low	high	Low	Low
Time synchronized data	Yes	Yes	No	No	Per stage
Particular PMU position	Yes	No	No	No	No
Single phase fault identification	No	No	No	Yes	Yes
Mix data from Other IED	No	No	potentially	No	Yes

Credit Author Statement

This research work has been financially supported by Dutch Scientific Council NWO through the project Resilient Synchro-phasor Grid Protection Platform

Declaration of Competing Interest

The authors declare that they have no known competing financial interests or personal relationships that could have appeared to influence the work reported in this paper.

References

[1] Z.Y. He, R.K. Mai, W. He, Q.Q. Qian, Phasor-measurement-unit-based transmission line fault location estimator under dynamic conditions, IET Trans. Dist. 5 (11) (2011) 1183–1191.

[2] A. Salehi-Dobakhshari, A.M. Ranjbar, Application of synchronized phasor measurements to wide-area fault diagnosis and location, IET Trans. Dist. 8 (4) (2014) 716–729.
[3] A.H. Al-Mohammed, M.A. Abido, A fully adaptive PMU-based fault location algorithm for series-compensated lines, IEEE Trans. Power Syst. 29 (5) (2014) 2129–2137.
[4] M. He, J. Zhang, A dependency graph approach for fault detection and localization towards secure smart grid, IEEE Trans. Smart Grid 2 (2) (2011) 342–351.
[5] A. Sharafi, M. Sanaye-Pasand, F. Aminifar, Transmission system wide-area back-up protection using current phasor measurements, Int. J. Elect. Power Energy Syst. 92 (2017) 93–103.
[6] F. Yu, C.D. Booth, A. Dysko, Voltage-based fault identification for PMU-based wide area backup protection scheme, in: Proceedings of the IEEE Power & Energy Society General Meeting, Chicago USA, 2017.
[7] C.J. Lee, J.B. Park, J.R. Shin, Z.M. Radojevie, A new two terminal numerical algorithm for fault location, distance protection, and arcing fault recognition, IEEE Trans. Power Syst. 21 (3) (2006) 1460–1462.
[8] A.G. Phadke, P. Wall, L. Ding, V. Terzija, Improving the performance of power system protection using wide area monitoring systems, J. Mod. Power Syst. Clean Energy 4 (3) (2016) 319–331.
[9] G. Kavya, M.M. Devi, M. Geethanjali, Wide area backup protection scheme using optimal PMUs, in: Proceedings of the National Power Energy Conference, Madurai India, 2018.
[10] I. Kamwa, A.K. Pradhan, G. Joos, Automatic segmentation of large power systems into fuzzy coherent areas for dynamic vulnerability assessment, IEEE Trans. Power Syst. 22 (4) (2007) 1974–1985.
[11] I. Kamwa, A.K. Pradhan, G. Joos, S.R. Samantaray, Fuzzy partitioning of a real power system for dynamic vulnerability assessment, IEEE Trans. Power Syst. 24 (3) (2009), 13561365.
[12] J. Ma, C. Liu, J.S. Thorp, A wide-area backup protection based on distance protection fitting factor, IEEE. Trans. Power Deliv. 31 (5) (2016) 2196–2205.
[13] M. Majidi, M. Etezadi-Amoli, M.S. Fadali, A sparse-data-driven approach for fault location in transmission networks, IEEE Trans. Smart Grid 8 (2) (2017) 548–556.
[14] J. Zare, F. Aminifar, M. Sanaye-Pasand, Communication-constrained regionalization of power systems for synchrophasor-based wide-area backup protection scheme, IEEE Trans. Smart Grid 6 (3) (2015) 1530–1538.
[15] P. Kundu, A.K. Pradhan, Power network protection using wide-area measurements considering uncertainty in data availability, IEEE Syst. J. 12 (4) (2018) 3358–3368.
[16] S. Azizi, M. Sanayed-Pasand, A straightforward method for wide-area fault location on transmission networks, IEEE Trans. Power Deliv. 30 (1) (2015) 264–272.
[17] S. Azizi, M. Sanayed-Pasand, From available synchrophasor data to short circuit fault identity: formulation and feasibility analysis, IEEE Trans. Power Syst. 32 (3) (2017) 2062–2071.
[18] S. Azizi, G. Liu, A.S. Dobakhshari, V. Terzija, Wide-area backup protection against asymmetrical faults using available phasor measurements, IEEE Trans. Power Deliv. 35 (4) (2020) 2032–2039.
[19] L. Xie, Y. Chen, P.R. Kumar, Dimensionality reduction of synchrophasor data for early event detection: linearized analysis, IEEE Trans. Power Syst. 29 (6) (2014) 2784–2794.
[20] A.S. Dobakhshari, Wide-area fault location of transmission lines by hybrid synchronized/unsynchronized voltage measurements, IEEE Trans. Smart Grid 9 (3) (2016) 1869–1877.
[21] P. Horton, S. Swain, Using superimposed principles (Delta) in protection techniques in an increasingly challenging power network, in: Proceedings of the 40th Annual Conference for Protective Relay Engineers (CPRE)., 2017.
[22] J. Kiusalaas, Numerical Methods in Engineering Using Matlab, Cambridge university press, UK, 2005.
[23] E. Price, T. Einarsson, The performance of faulted phase selectors used in transmission line distance applications, in: Proceedings of the 61st Annual Conference for Protective Relays Engineers (CPRE), 2018.
[24] J. Roberts, A. Guzman, Directional element design and evaluation, in: Proceedings of the 21st Annual Western Protective Relay Conference, Washington, 1994.
[25] N. Fischer, G. Benmouyal, D. Hou, D. Tziouvaras, J. Byrne-Finley, B. Smyth, Tutorial on power swing blocking and out-of-step tripping, in: Proceedings of the 39th Annual Western Protective Relay Conference, Washington, 2012.